Journal of Sound and Vibration 326 (2009) 489–502

Contents lists available at ScienceDirect

Journal of Sound and Vibration

journal homepage: www.elsevier.com/locate/jsvi

Construction and characterization of a particle-based thrust damping system

Binoy M. Shah [a], Davy Pillet [b], Xian-Ming Bai [c], Leon M. Keer [a,*], Q. Jane Wang [a], Randall Q. Snurr [c]

[a] Department of Mechanical Engineering, Northwestern University, 2145 Sheridan Road, Evanston, IL 60208-3109, USA
[b] Department of Mechanical Engineering, École Polytechnique, 91128 Paliseau, France
[c] Department of Chemical and Biological Engineering, Northwestern University, Evanston, IL 60208, USA

ARTICLE INFO

Article history:
Received 29 March 2009
Received in revised form
3 June 2009
Accepted 5 June 2009
Handling Editor: C.L. Morfey

ABSTRACT

A particle-based thrust damping system is presented which considers a piston oscillating in a dry particle medium to dissipate energy through friction and inelastic collisions. An experimental setup is designed to evaluate the influence of particle properties and device parameters on damping performance. Particle properties such as size (15 nm–3 mm), mass and temperature (20–130 °C) are evaluated in addition to device parameters such as container size and the piston's start position. These results demonstrate the effectiveness of this new particle damping method and provide insights that may be useful in the development of future particle damping technologies.

1. Introduction

Damping devices are widely used in aerospace, automotive and structural applications for shock, vibration and force absorption. They function to provide stability and control to a dynamic mechanical system by converting excess mechanical energy into heat [1]. Dampers are often required to be reliable in harsh environments and function in the presence of extreme temperature variations, vacuum conditions and zero to high gravitational forces for high performance applications.

Current damping technology uses either fluid or mechanical means to achieve damping, but both have limitations. Fluid-based dampers use shear and displacement of a viscous fluid to dissipate energy, while mechanical dampers use either the hysterisis of viscoelastic materials or the friction between contacting surfaces [1]. The viscosity of fluids varies significantly with temperature, making damping unreliable when temperature changes [2]. On the other hand, mechanical dampers under cyclical loading are vulnerable to material degradation and life-threatening fatigue.

A particle-based damping system can overcome some limitations by using particles as the damping medium and inter-particle interaction as the damping mechanism. The dual solid- and liquid-like properties of a particle medium provide the system with two unique advantages: (i) the solid-like properties can enable temperature independence, and (ii) the liquid-like properties can allow for flow and reorganization of particles to facilitate fatigue-free performance [3,4].

Particle damping is affected by three main factors: particle flow behavior, packing density and granular stress. These factors can be influenced by controlling the particle's surface and bulk properties, and damping device parameters [5]. Particle surface properties are controlled by particle size, shape, surface energy, interstitial fluid, coefficient of friction, and

* Corresponding author. Tel.: +1 847 491 4046.
E-mail address: l-keer@northwestern.edu (L.M. Keer).

0022-460X/$ - see front matter © 2009 Elsevier Ltd. All rights reserved.
doi:10.1016/j.jsv.2009.06.007

temperature. The bulk properties are controlled by particle mass, elastic modulus and coefficient of restitution. Damping device parameters consist of particle container size, fill volume and vibration characteristics, e.g. amplitude, frequency and direction of vibration relative to the gravity field.

Experimental [5–18] and analytical [12,19] research in particle damping has primarily been in the area of impact damping where particles are filled into one or many containers and forced into horizontal or vertical vibration. Energy is dissipated through friction and collision among particles as well as between particles and container walls. For example, damping was applied to a cantilever beam by drilling multiple small diameter holes, and filling them with particles [5]. Another experimental method used a particle filled container mounted on top of a vibrating structure to attenuate its vibrations [10,16]. Damping behavior of particles ranging in size from 45 μm to 12.7 mm and made of various materials (aluminum, glass, lead, stainless steel, tungsten, titanium etc.), have been studied. In addition, the effect of container size, mass ratio and the level of excitation have also been investigated [10]. It was observed that the effect of particle size was coupled with the size of the container and the level of excitation. As particle size decreased, the influence of the container size and the intensity of the excitation decreased. Damping became inefficient as the ratio of the total mass of the particles increased with respect to the mass of the vibrating structure [16]. Impact damping using a vertically vibrating container under free vibrations was found to be very effective, highly non-linear and one order greater in magnitude than the intrinsic material damping of structural metals [6,12]. Simulations of such systems were performed using the Discrete Element Method for granular assemblies [16–22]. Several patents have also been awarded for various multi-particle impact damping ideas [23–26].

The impact damping method has two limitations. First, damping does not occur at low frequencies where the acceleration of the container is lower than that of gravity because the particles lack sufficient energy to begin colliding with each other and instead they move as one lumped mass [14,19]. Second, the damping capabilities are dependent on the quantity and mass of free particles available for collisions. The tendency of particles to self-assemble into a packed configuration under vibration can reduce the availability of free particles and therefore decrease damping effectiveness [5]. All the particle-based damping studies so far have primarily focused on damping due to particle collisions in a closed container. Damping produced by the interaction of a vertically vibrating object in a stationary particle bed has not been investigated. In addition, particles in the size range from millimeters to micrometers have been studied, but the performance of nano-particles in damping applications has not been explored.

This paper introduces a new particle-based thrust-damping system. Damping in the system is produced by the resistance force experienced by a piston which oscillates in a container filled with dry particle medium. The paper is organized as follows: the experimental setup is described in Section 2, the method of analysis is presented in Section 3, and the role of particle properties and device parameters on damping performance are provided in Section 4.

2. Description of experimental setup

A free vibrating mass–spring-damper system was built to experimentally characterize the particle-produced damping. The experimental setup of the system is shown in Fig. 1a and its equivalent model is illustrated in Fig. 1b. This system has the form of a thrust damper in which a piston vibrates vertically in a damping medium. The free vibration damping is characterized by measuring its displacement decay.

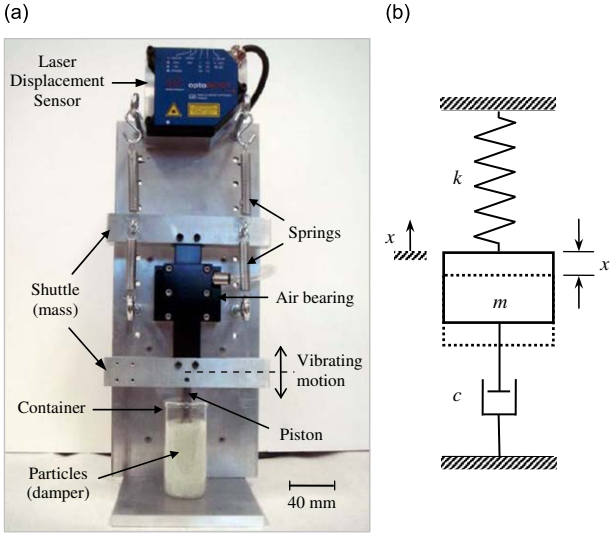

Fig. 1. (a) Experimental setup designed to measure thrust damping, and (b) its equivalent system model in which k is the stiffness, m the mass, c the damping coefficient, and x the displacement of the mass from its equilibrium position.

In the experimental setup, a shuttle slides up and down on a linear rectangular air bearing, which guides the shuttle in frictionless motion constrained in the vertical direction. Four extension springs are connected in parallel and attached to the shuttle to produce an undamped system of stiffness $k_n = 1985$ N/m. A particle bed consisting of the damping media is held in a glass container. A cylindrical steel rod is used as the thrust piston with its top end attached to the bottom of the shuttle and the bottom end immersed into the particle bed. The sum of the weights of the shuttle and the piston is $m = 0.7$ kg (Fig. 1(b)). The drag force exerted by the particle bed on the vibrating piston produces damping. In absence of the damping medium, the system is referred to as undamped. Nevertheless, the system still has inherent damping caused by factors such as internal friction and air resistance. A laser displacement sensor with displacement resolution of 1 μm and measurement frequency of 2500 Hz is used to measure the oscillations of the shuttle as a function of time t.

In this study, particles ranging from nano-scale to macro-scale were used as the damping media, e.g. silica with average diameter $d = 15 \pm 5$ nm (Sigma Aldrich), glass with $d = 50 \pm 10$ μm (Jaygo and 3 M) and $d = 1, 2, 3 \pm 0.1$ mm (Fox Industries), as well as steel particles with $d = 1, 2 \pm 0.1$ mm (Fox Industries). The images of some sample particles are shown in Fig. 2 and their physical properties are presented in Table 1. Particles were selected based on their shape, size and material properties. Glass and steel were selected because they are widely used, well characterized and strong enough to endure repeated loadings. With their melting points greater than 1400 °C, these particles can also sustain high temperatures. Particles were chosen to be smooth and spherical in order to ensure consistent particle packing and flow behavior.

The experiments described in this paper were all conducted using the following procedure. Each experiment was prepared by arranging the piston and the particle bed in the configuration as shown in Fig. 3. A reproducible particle bed was created by pouring the particles into a cylindrical glass container of inner diameter D_c and filling it to a column height of H. The particles were then stirred to create uniform random packing. The top of the particle bed is considered as a free surface, as no constraints were applied there. The steel piston of diameter D_p was immersed into the particle bed to a depth of L from the free surface and given an initial downward or upward displacement A_0 to provide initial potential energy to the system. The piston was then released and set into free vibration which was recorded by the laser. The ambient relative humidity during the experiments was 24 ± 3%. Unless mentioned otherwise, the standard parameters used for experiments

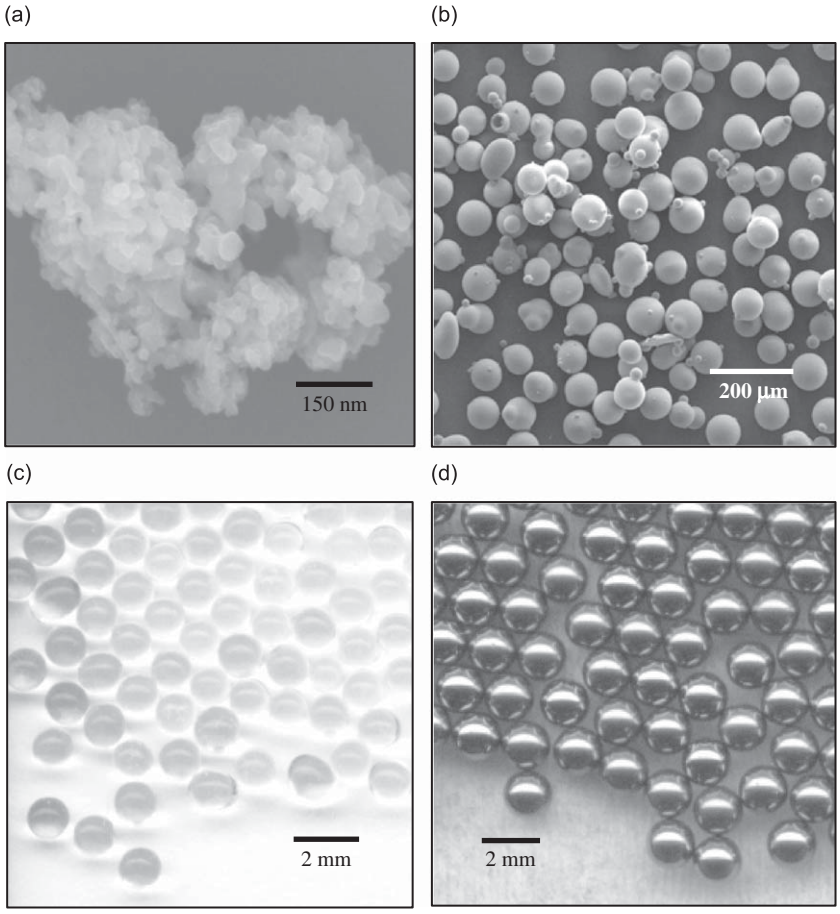

Fig. 2. Images of some particles used as the damping media: (a) 15 nm silica, (b) 50 μm glass, (c) 1 mm glass, and (d) 1 mm steel. The images were captured using scanning electron microscopy and optical microscopy.

Table 1
Physical properties of silica, glass and steel particles used in the experiments.

Material	Silica	Glass	Steel
Size scale (diameter d)	Nano (15 nm)	Micro (50 μm), Macro (1, 2, and 3 mm)	Macro (1 and 2 mm)
Density ρ (kg/m^3)	2500	250, 1550	7800
Young's modulus E (Gpa)	94	63	193

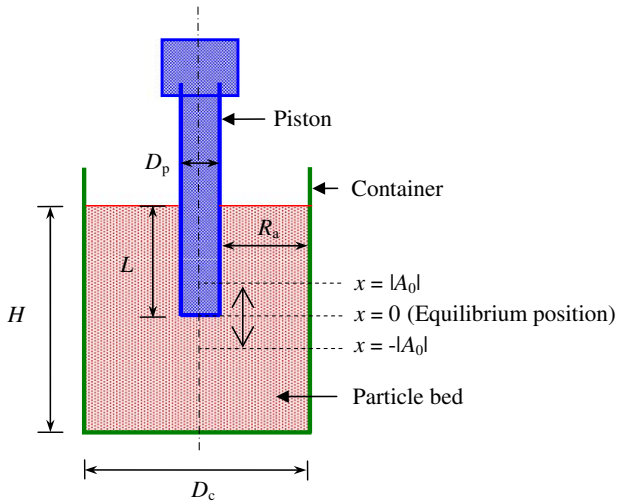

Fig. 3. Schematic of the piston, the particle bed, and the container as configured in the experimental setup.

are as follows: $H = 70$, $L = 35$, $D_c = 54.6$, $D_p = 9.5$, and $A_0 = -10$ mm. A particle dynamics based simulation system configured to model the experimental setup is presented in Ref. [20].

3. Method of analysis

This section presents the notation and methodology used in the analysis of the experimental data. Fig. 4 shows the displacement decay of a damped free vibrating system. The displacement of the piston is a function of time t and denoted by $x(t)$. The variables t_i^α are used to denote the discrete moments when $x(t)$ reaches its valley value ($\alpha = 1$) and peak value ($\alpha = 2$) during the i-th cycle for all $i \geq 1$. The system vibrates with a constant period, $\Delta t_i^\alpha = t_i^\alpha - t_{i-1}^\alpha$ and the frequency is obtained from $f = 1/\Delta t_i^\alpha = \sqrt{k/m}/(2\pi)$. Each cycle is comprised of a pair of up-stroke and down-stroke motions. Given the initial displacement as shown in Fig. 4, a motion from $x(t_i^1)$ to $x(t_i^2)$ is called *up-stroke* and a motion from $x(t_i^2)$ to $x(t_{i+1}^1)$ is *down-stroke*.

In general, damping models are classified into two categories: viscous and frictional [1]. If the displacement $x(t_i^\alpha)$ demonstrates an exponential decay and the damped frequency f_d is less than the undamped frequency f_n, the damping is considered as viscous. In contrast, if $x(t_i^\alpha)$ demonstrates a linear decay and $f_d = f_n$, the damping is frictional.

However, as explained in Section 4.1, damping in the present system is non-linear and therefore cannot be simply described by either a viscous or a frictional model. Instead, the principle of energy conservation is used to describe the experimental data. Accordingly, the total energy $E(t)$ of a system is equal to the sum of potential energy $U(t)$ and kinetic energy $K(t)$, i.e., $E(t) = U(t) + K(t)$. At the moments when $t = t_i^\alpha$, the velocity is zero, and therefore the kinetic energy is zero. As a result, the energy in the system is

$$E(t_i^\alpha) = \tfrac{1}{2} k x^2(t_i^\alpha). \tag{1}$$

The energy lost within one cycle is obtained by

$$W(t_i^\alpha) = E(t_i^\alpha) - E(t_{i+1}^\alpha) \tag{2}$$

and the ratio of energy lost per cycle to the initial system energy is $W(t_i^\alpha)/E(t_1^\alpha)$. The damping efficiency per cycle is given by the specific damping capacity $\Psi(t_i^\alpha)$. It is the ratio of the energy lost within one cycle to the energy at the start of the

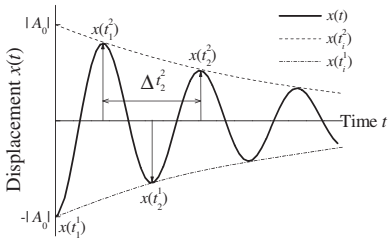

Fig. 4. Schematic of the displacement decay in a damped free vibrating system.

cycle as follows

$$\Psi(t_i^\alpha) = \frac{W(t_i^\alpha)}{E(t_i^\alpha)} = \frac{x^2(t_i^\alpha) - x^2(t_{i+1}^\alpha)}{x^2(t_i^\alpha)}. \tag{3}$$

A decay time constant τ is used as a measure of the overall damping effectiveness. We define the value of τ as the time required for the system to reach $1/e$ of the initial energy $E(t_1^\alpha)$.

4. Results

This section presents the performance characteristics of the thrust-damping method. Displacement and energy decay for 1 mm glass media are analyzed to quantify the characteristics of the experimental setup. Furthermore, the role of particle properties, i.e. size, mass and temperature, as well as device parameters, such as particle container size and piston's start position, on such damping factors as particle flow behavior, packing density and granular stress are examined.

4.1. Damping with 1 mm glass particles

A damping experiment under free vibrations was conducted using 1 mm diameter glass particles. The vibrations were measured and the energy decay computed. The displacements $x(t)$ of the piston for a particle-damped and an undamped response are shown in Fig. 5. The displacement decay of the undamped system is negligible. The frequency for the damped system is $f_d = 8.82$ Hz and for the undamped system is $f_n = 8.47$ Hz., i.e., $f_d > f_n$ by 0.35 Hz or 4%. This frequency behavior is an unusual characteristic for a damping system. Generally $f_d < f_n$ in a particle-based impact damping or a fluid-based viscous damping system, and $f_d = f_n$ in a frictional damping system [1,12]. The increase in frequency is caused by either an increase in the stiffness k of the system or a decrease in the mass m. Since the mass is constant at $m = 0.7$ kg, the stiffness of the damped system ($k_d = 2150$ N/m) is 165 N/m or 8% greater than that of the undamped system ($k_n = 1985$ N/m). This implies that the stiffness of individual particles and the piston's motion in the particle bed can increase the damped frequency by increasing the overall stiffness of the system.

The amplitudes $x(t_i^\alpha)$ at the minimum ($\alpha = 1$) and maximum ($\alpha = 2$) displacements are presented in Fig. 6a as the absolute value of the amplitude per stroke $|x(t_i^\alpha)|$. A stepwise trend in the amplitude decay was observed for consecutive up- and down-strokes of the piston. The change in amplitude was large during down-strokes but negligible during the up-strokes, which implies that damping did not occur equally throughout the duration of one cycle, but rather took place primarily during the downstroke of the piston. Such stepwise decay occurred due to the combination of two experimental conditions. First, the bottom of the particle bed was limited in its displacement by the rigid container wall while the top was a free surface since no constraints were applied to it. Second, the motion of the piston was parallel to the gravity vector. Under the influence of these two conditions, the piston experienced a large resistance during the downstroke caused by localized stresses in the particle bed [27], and a small resistance during the upstroke caused by friction between the piston and the particles.

The amplitude decay per cycle for the displacement $x(t_i^1)$ in Fig. 6b shows that the decay is rapid; the initial amplitude A_0 is reduced by 50% in four cycles. In order to find the trend of the decay, $x(t_i^1)$ was fitted by an exponential and a linear function. As shown in Fig. 6a, neither function matched the decay trend. In addition, due to the unusual characteristic of the frequency, i.e., $f_d > f_n$, neither a viscous nor a frictional model could be used to describe the damping behavior. Therefore the use of a conventional damping factor to quantify the damping rate is not possible and damping appears to be non-linear. Instead, the critical decay time, based on the energy conservation principle, described in Section 3, is used to quantify the damping rate.

Fig. 7a studies the ratio of energy at the beginning of each cycle to the initial energy of the system $E(t_i^\alpha)/E(t_1^\alpha)$ for $\alpha = 1$. The initial energy $E(t_1^1) = 107.5$ mJ for $|A_0| = 10$ mm and $k_d = 2150$ N/m. The critical decay time can be identified as $\tau = 0.36$ s, which is the time required to dissipate 63.3% of $E(t_1^1)$. Fig. 7b shows that the energy lost per cycle $W(t_i^\alpha)$ is reduced by an order of magnitude from 27.6 to 2.6 mJ in the first eight cycles. In comparison, the un-damped system loses a constant 0.7 mJ per cycle. Fig. 7c plots the specific damping capacity $\Psi(t_i^\alpha)$, against the non-dimensional acceleration given

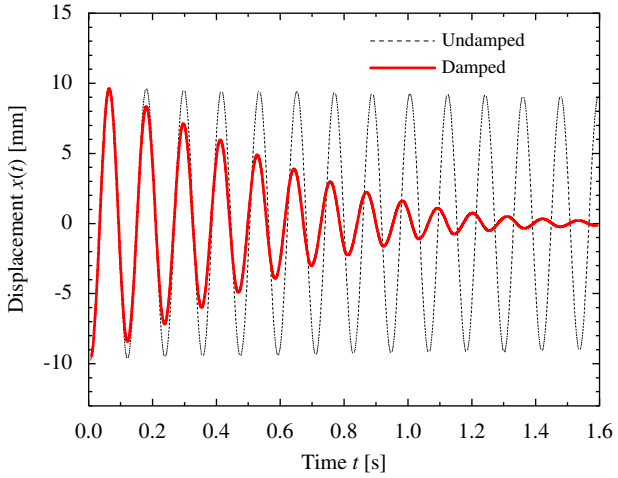

Fig. 5. Displacement of the piston in a particle-damped (1 mm glass) and an undamped system under free vibration.

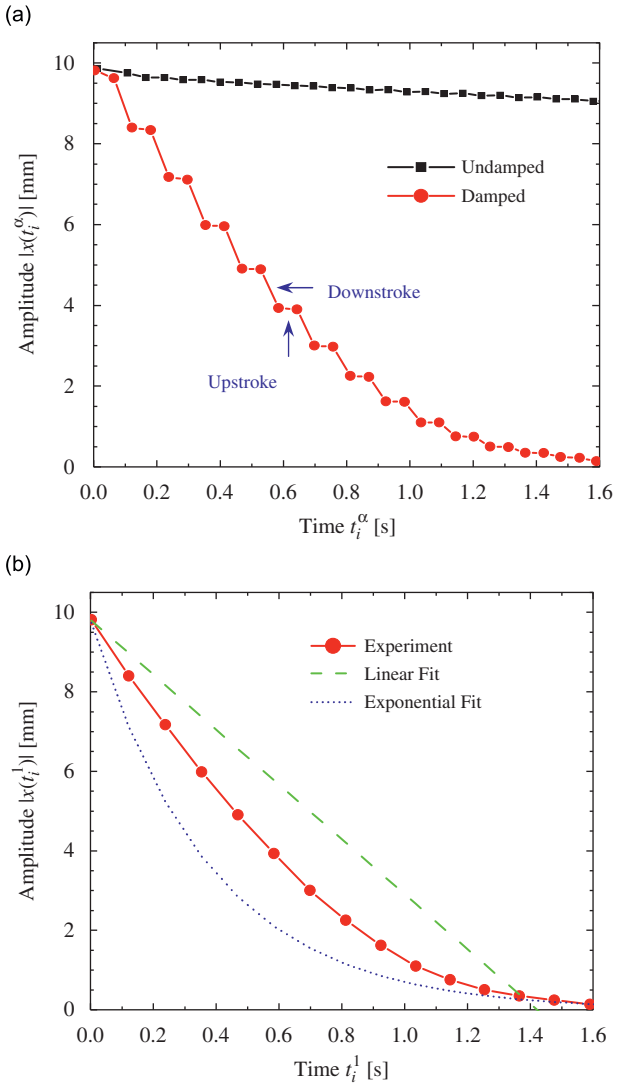

Fig. 6. Displacement trends for damping with 1 mm glass particles: (a) amplitude decay per stroke for the damped and the un-damped system, and (b) amplitude decay per cycle in comparison with its exponential and linear fit.

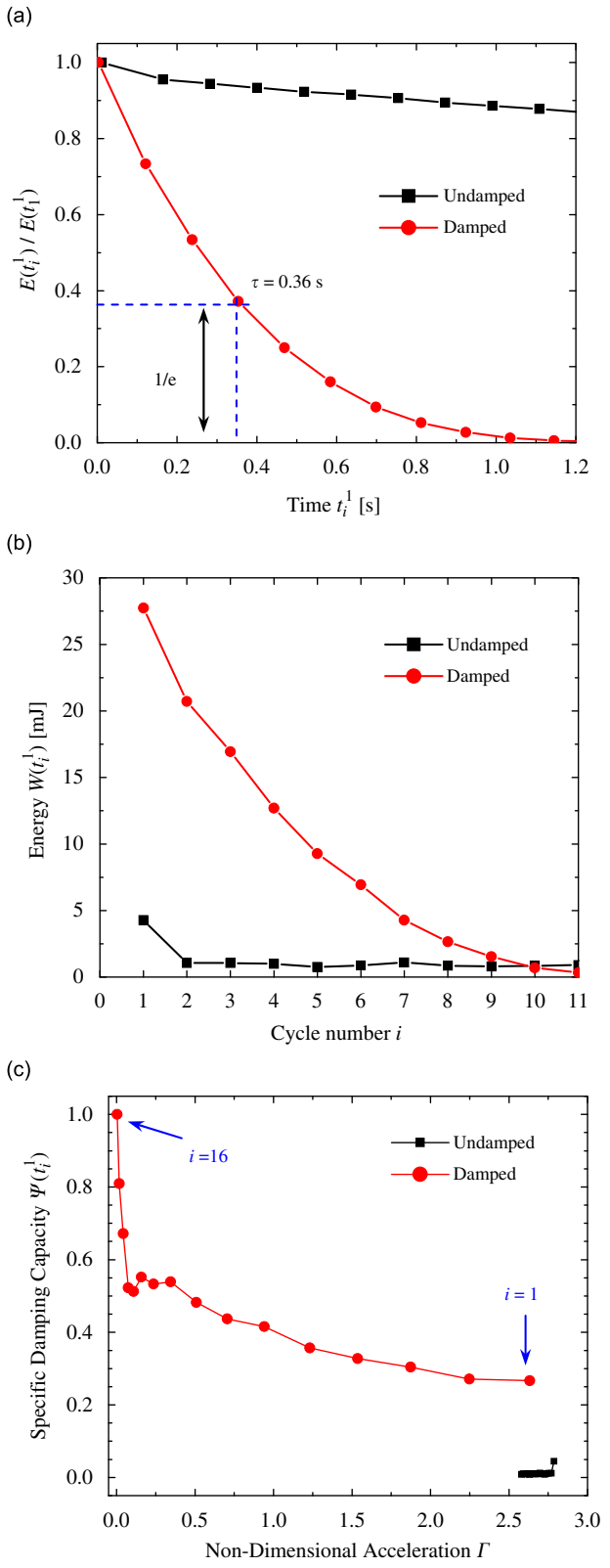

Fig. 7. Energy trends for damping with 1 mm glass particles: (a) ratio of energy at the start of a cycle to the initial system energy, shown along with the critical decay time τ (b) energy lost per cycle $W(t_i^z)$, and (c) the specific damping capacity $\Psi(t_i^z)$.

by $\Gamma = (2\pi f_d)^2 x(t_i^1)/g$, where g is the acceleration due to gravity. It shows that the thrust-damping system can achieve high damping capacity even under low excitation levels where $\Gamma < 1$, which is not possible for an impact damping system [19].

4.2. Effect of particle size

The size of a particle determines the magnitude of its surface and body forces. The competition between these two forces affects the flow characteristics and thereby the damping performance. Damping experiments were conducted with particles of three different length scales, i.e. nanometer, micrometer and millimeter, in order to investigate the size effect. Particles of silica with $d = 15$ nm, and glass with $d = 50$ μm, 1 mm and 3 mm were used in the experiments.

The amplitude decay for various particle sizes is presented in Fig. 8. A size effect can be clearly observed which shows that because of cohesive forces, damping is negligible with 15 nm particles but significantly greater with 1 mm and 3 mm particles. The difference in the damping rate between 1 mm and 3 mm particles is very small but that between 15 nm and 50 μm particles is very large. In addition, damping rate decreases noticeably as the amplitude for the 3 mm particles drops below the particle size.

The weak damping performance of the 15 nm particles can be explained based on the following experimental observation. During the first down-stroke, as the piston entered the particle bed, the particles compacted together in the area between the piston and the container wall. As the piston moved out of the particle bed during the upstroke, the compacted particles retained their position and created a void about the size of the piston. The gravity force was unable to overcome the inter-particle cohesive force in order to reorganize the particles and fill the void. Therefore, during the second down-stroke, the piston entered the void created previously and encountered no noticeable resistance. Although nano-particles appear to be ineffective in this thrust-damping configuration, their ability to self-assemble into complex agglomerate structure provides them the potential to dissipate energy by fracturing their numerous inter-particle bonds [22,28].

The experimental observation suggests that the flow-ability of particles has a significant influence on the damping performance. A particle's flow regime can be identified using a non-dimensional cohesive granular bond number Bo_g. It is the ratio of two competing forces experienced by particles: inter-particle adhesion F_{ad} and gravity F_g [29]. The bond number Bo_g for a perfect sphere is

$$Bo_g = \frac{F_{ad}}{F_g} = \left(\frac{A_H}{4\pi\rho g z^2}\right) \cdot \left(\frac{1}{d^2}\right) \tag{4}$$

Here F_{ad} is represented by the van der Waals force F_{vdW} which is a molecular level force that is always present between two surfaces but drops off rapidly for surfaces separated by more than 10 nm [30]. The force is denoted by $F_{vdw} = (A_H d)/(24z^2)$ where A_H is Hamaker's constant of a material, d the particle diameter, and z the separation distance between the surfaces of two particles. In addition, other inter-particle forces such as capillary, produced by the presence of interstitial fluid between particles, and electrostatic, produced by electrical charges on particle surface, can also influence F_{ad}. However, capillary forces can be neglected for a dry particle system and charging due to tribo-electrification can also be considered negligible between particles in a system where all the particles are made of the same material [31]. For particles with rough surfaces or irregular shapes, F_{vdW} and therefore Bo_g can be significantly lower in magnitude

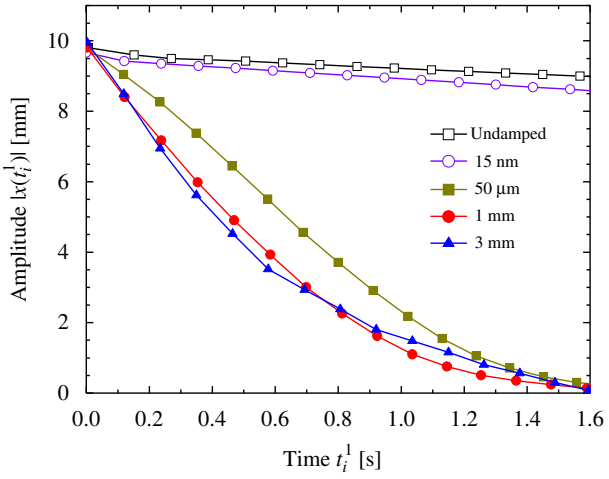

Fig. 8. Amplitude decay per cycle showing the effect of particle size on damping performance.

Table 2
Critical decay time τ and the granular cohesive bond number Bo_g for particles of four sizes. The value of $Bo_g \gg 1$ implies that the particles are very cohesive. Such particles have low damping effectiveness as indicated by the large τ values.

Particle size (d)	Critical decay time τ (s)	Cohesive bond number BO_g
Damped		
Glass (3 mm)	0.31	0.15
Glass (1 mm)	0.36	1.3
Glass (50 μm)	0.52	520
Silica (15 nm)	5.05	3.6×10^9
Undamped		
N/A	6.80	N/A

depending on the size of the surface asperities [32]. In addition Bo_g is also a function of particle density and therefore affected by particle mass.

Table 2 compares the critical decay time τ to Bo_g for the four particles tested, assuming $A_H = 10^{-20}$ J and $z = 0.2$ nm. The transition between cohesive and free-flowing particles is indicated by $Bo_g = 1$. For a particle such as 15 nm silica with $Bo_g \gg 1$, cohesive force is dominant and flow-ability is limited. Such particles demonstrate reduced effectiveness in thrust damping as indicated by the large decay time. On the other hand, when $Bo_g < 1$, as in the case of 3 mm particles, gravity force dominates, allowing for free-flow and reorganization of particles. Such particles enable very effective damping. In addition, the damping rate is more sensitive to variations in particle size at the nanometer and micrometer range than at the millimeter range. Furthermore, the bond number Bo_g can be a useful indicator in identifying the damping effectiveness of particles based on their cohesive flow properties.

4.3. Effect of particle mass

The mass of a particle can influence the particle flow behavior as well as the stress in the particle bed. Two experiments were conducted to investigate the effect of particle mass on the damping performance. Heavy and light weight spherical particles of equal diameters were selected for comparison. Particles with $d = 50$ μm were used in the first experiment and with $d = 2$ mm in the second one.

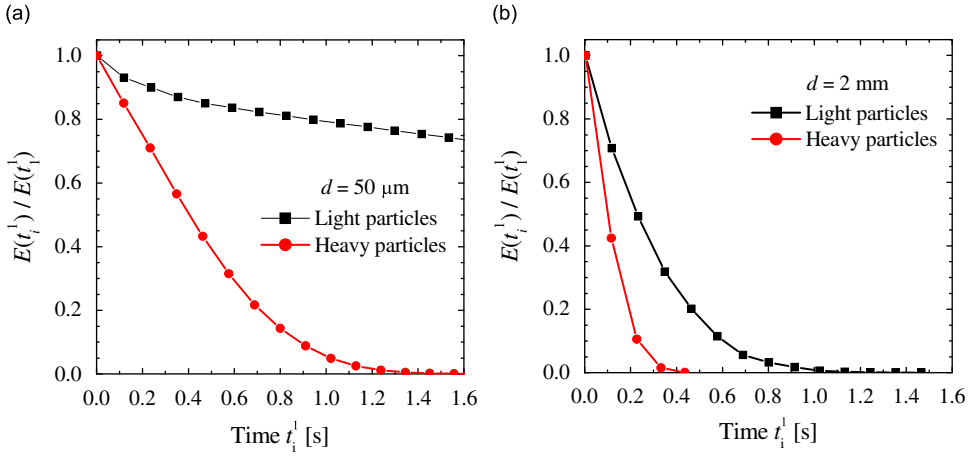

Fig. 9. Comparison of energy decay between light and heavy particles of diameter 50 μm (a) and 2 mm (b).

For the case with $d = 50$ μm, solid glass spheres with density $\rho = 1550$ kg/m^3 were used as heavy particles and hollow glass spheres with $\rho = 250$ kg/m^3 as light particles. For the case with $d = 2$ mm, all the particles were spherical solids. Steel particles with $\rho = 7800$ kg/m^3 were used as the heavy ones, while glass with $\rho = 1550$ kg/m^3 as the lighter ones.

Fig. 9 presents the energy decays for the two experiments and shows that the heavier particles dissipate energy faster than lighter ones for both particle sizes. In the case of $d = 50$ μm, $\tau = 0.52$ s for heavier particles and $\tau \sim 5.0$ s for the lighter ones. A ten fold increase in the damping rate is achieved by a six fold increase in particle weight. The lighter micro-particles have the same negligible damping rate, i.e. $\tau \sim 5.0$ s, as that of the cohesive 15 nm silica particles (Table 2). In the case of $d = 2$ mm, $\tau = 0.14$ s for the heavier particles and $\tau = 0.32$ s for the lighter ones. A five fold increase in the particle weight only doubled the damping rate. Similar results have been found using particle dynamics simulations [20]. This

demonstrates that the particle mass has a significant affect on damping; however, damping is much more sensitive to particle mass for particles in the micrometer scale than in the millimeter scale.

4.4. Effect of temperature

The primary advantage of a particle-damping medium is its ability to provide temperature independent damping. While the damping performance of a dry particle medium unlike a viscous fluid is said to be unaffected by large temperature variations [5,6], apparently no experimental evidence has been reported in the literature. In this section, we experimentally evaluate the damping at temperatures ranging from 20 to 130 °C.

Glass particles of two different sizes, $d = 50\,\mu m$ and $d = 1$ mm, were used for evaluation. Experimental parameters were set to $A_0 = -5$ mm and $L = 25$ mm. The particles were filled in a container, heated to 130 °C and stirred to ensure uniform heating. Damping tests were performed periodically as the particles cooled from 130 to 20 °C at 40% relative humidity. The temperature T in the particle bed was continuously monitored. For each particle size, 47 damping tests were conducted over the entire temperature range. The damping performance for each test was evaluated in terms of the critical decay time τ. The results are shown in Fig. 10 as τ versus T for both particle sizes over the 110° temperature range.

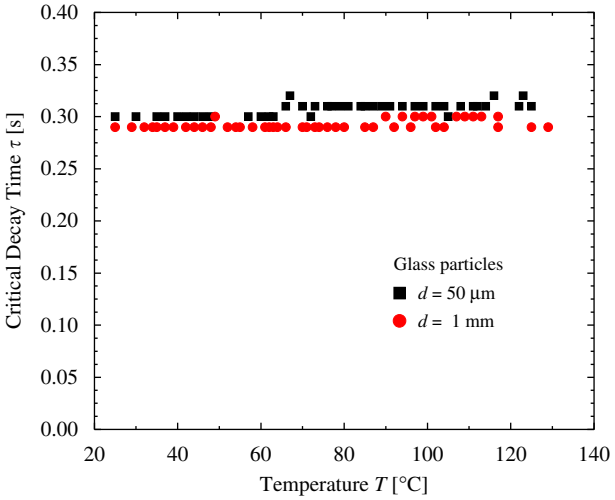

Fig. 10. Effect of operating temperature on the damping performance of 50 μm and 1 mm diameter glass particles.

The figure indicates that the damping performance is constant over the entire temperature range with negligible variations. The average value of τ for the 1 mm particles is 0.29 s with a standard deviation $\sigma = 0.0036$. For the 50 μm particles, τ is 0.31 s with $\sigma = 0.0062$. Such small values of σ indicate that the damping performance is temperature independent at both micrometer and millimeter scales. The temperature independence of a particle is limited by the melting point of its material. Therefore, materials with high melting point e.g., titanium dioxide (1870 °C) or tungsten carbide (2870 °C), can be used for extreme high temperature applications.

Fig. 10 also illustrates the repeatability i.e. history independence, in this particle damping system. The fact that τ does not vary with consecutive tests suggests that the particle bed does not retain any memory from its previous tests that can influence its future tests. This history independent feature shows the potential for the particle damping system not just for one-time use applications, but also for multiple or continuous shock absorption.

4.5. Effect of particle container size

The size of the particle container, particularly its diameter, determines the physical dimensions of particle bed and the granular stress in it. The stress is dependent upon the annulus spacing $R_a = (D_c - D_p)/2$ as shown in Fig. 3. For each value of $R_a = 5.25$, 15.25, 25.25, 35.25 and 45.25 mm, damping tests were conducted using glass particles with $d = 1$ mm. The corresponding container sizes have $D_c = 20$, 40, 60, 80 and 100 mm and piston has $D_p = 9.5$ mm. The height H of the particle bed and the immersion depth L of the piston were kept constant at 70 and 35 mm, respectively. Fig. 11 presents $W(t_i^1)/E(t_1^1)$ i.e., the ratio of energy lost per cycle to the initial system energy, for the five R_a values.

Damping was almost the same for all values of $R_a \geq 15.25$ mm, for each of which about 40% to 50% of initial energy was lost within the first cycle. However, damping was extremely high when the confinement of the particle bed was reduced to $R_a = 5.25$ mm, for which more than 99% of the initial energy was dissipated within the first down-stroke alone. In such a small confinement, the container wall influences the motion of the piston by inducing large stress in the particle bed and

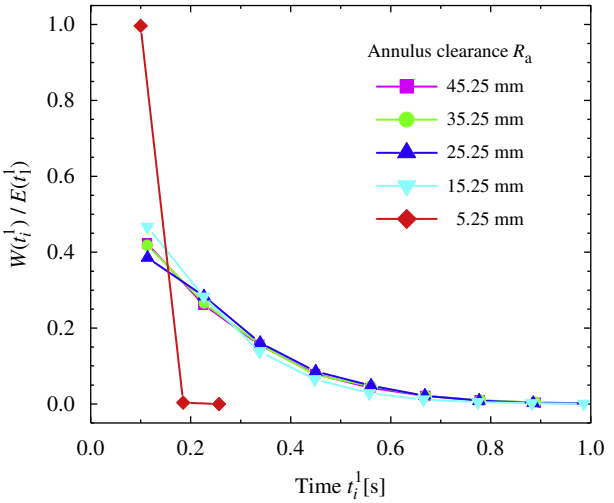

Fig. 11. The effect of annulus size on damping shown as the ratio of energy lost per cycle to the initial system energy for 1 mm glass particles.

creating strong interlocking between particles [27]. When the force required to break this interlocking exceeds the penetration force of the piston, the motion of the piston is constricted and it is considered to be jammed. The jammed state is not desired because it abruptly stops the vibrations, thus causing damage to the system.

Interestingly, particles 20 times smaller in diameter i.e., $d = 50\,\mu$m displayed similar behavior as $d = 1$ mm except for the following difference. In the case of $R_a = 5.25$ mm, damping was very high but jamming did not occur. About 75% of initial energy was lost in the first cycle, which was lower than 99% as observed for $d = 1$ mm. This implies that for the two particle sizes, when $R_a < 15.25$ mm, either the granular stress around the piston is different or that the particles of different sizes behave differently under the same applied stress.

The experiments suggest that the optimal container size should be based on the annulus radius R_a of a particle bed, which for this configuration is between 5.25 and 15.25 mm. Unwanted jamming effects occur for $R_a \leq 5.25$ mm, while $R_a > 15.25$ mm does not provide any additional damping but rather adds unnecessary particle mass to the system.

4.6. *Effect of piston's start position*

This section investigates the sensitivity of damping to the start position of the piston based on three key parameters: (1) the immersion depth L of the piston's equilibrium position, (2) the sign of the amplitude A_0 with respect to the equilibrium ($A_0 = 0$), and (3) the magnitude $|A_0|$of the amplitude.

The immersion depth L is the distance between the top of the particle bed to the tip of the immersed piston when it is in its equilibrium position (Fig. 3). As L increases, for a given particle bed height H, the distance between the piston tip and the container bottom decreases and the total mass of the particles above the piston tip increases. Damping experiments with five immersion depths i.e., $L = 25$, 35, 45, 55 and 65 mm, were conducted using 1 mm glass particles, $H = 70$ mm and $A_0 = -5$ mm. Fig. 12 shows that damping increases steadily with immersion depth, suggesting that the granular stress around the piston tip also increases with L. A shallow depth of $L = 25$ mm produced low damping ($\tau = 0.31$ s) and a large depth of $L = 65$ mm produced high damping ($\tau = 0.09$ s). In the latter case, the piston tip touched the bottom wall of the container when an initial amplitude $A_0 = -5$ mm was provided. However, even at such close proximity to the bottom wall, no jamming effects were observed.

The effect of the sign of the amplitude was studied by comparing two cases: (1) piston displacements starting from above the equilibrium position ($A_0 > 0$) and (2) displacements starting from below ($A_0 < 0$). In both cases, the immersion depth was set at $L = 35$ mm, and the initial amplitude at $A_0 = 10$ mm and $A_0 = -10$ mm. The first stroke in the vibration with $A_0 < 0$ is an upstroke while the first one with $A_0 > 0$ is a downstroke. Fig. 13 compares the amplitude per stoke normalized by the initial amplitude for both the cases. Damping was found to be appreciably greater in the case of $A_0 > 0$, primarily caused by the difference in the damping during the downstroke S1 versus the downstroke S2, labeled in the Fig. 13. Even though both strokes started with about same initial energy of about 107 mJ, and both were the first downstrokes in their respective vibrations, nevertheless 77% of $E(t_1^1)$ was dissipated during S1 while only 22% was dissipated during S2, which suggests that two downstrokes with the same initial energy do not necessarily dissipate the same amount of energy. The difference between the two strokes stems from the fact that S1 was the first stroke while S2 was preceded by an upstroke. During S1, as the piston descended into a fresh particle bed, a dense packing arrangement was formed below the piston tip, which exerted a high resistance force. In comparison, lower resistance was exerted during S2 because it was

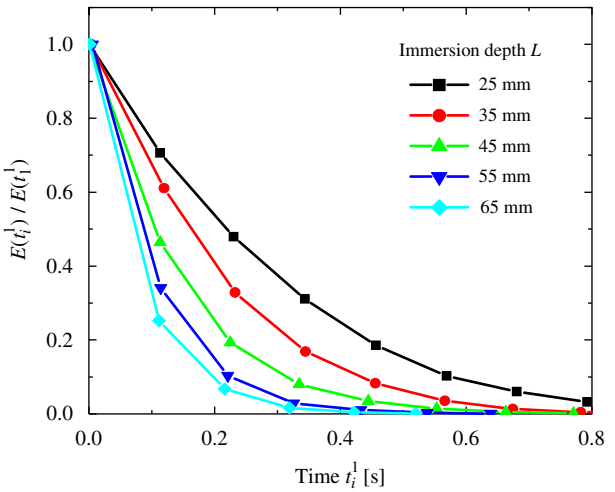

Fig. 12. Effect of variation in the piston immersion depth L, measured from the top of the particle bed, on damping with 1 mm glass particles shown as the ratio of energy remaining per cycle to the initial system energy. Damping increases steadily showing that the granular stress around the piston tip increases with L.

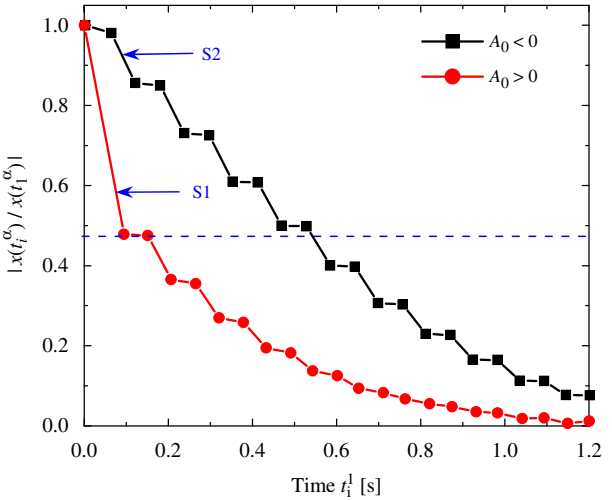

Fig. 13. Amplitude decay per stroke for two cases: $A_0 > 0$ and $A_0 < 0$. The first downstroke for each case is indicted by S1 and S2, respectively. The dashed line marks the amplitude at the end of the first upstroke for the case $A_0 > 0$ and shows that the decay rates are similar in the two cases below the line.

preceded by an upstroke that reorganized the particles and reduced their packing density under the piston tip. This phenomenon occurs for any downstroke that is preceded by an upstroke. It appears that the first upstroke in a vibration reorganizes the particles and erases their existing memory such that the amplitude decay rates thereafter are similar for two strokes starting with the same amplitude. For example, the amplitude decay rates between the two cases are similar below the dashed line marks the amplitude at the end of the first upstroke for $A_0 > 0$ in Fig. 13.

The magnitude $|A_0|$ of the initial amplitude also has an affect on the damping rate. Displacement decays $x(t)$ are compared for damping with two different values of $|A_0|$ in the cases where $A_0 < 0$ and when $A_0 > 0$. Fig. 14a compares $x(t)$ for $A_0 = -10$ mm (dotted curve) and $A_0 = -5$ mm (solid curve) and Fig. 14b compares $x(t)$ for $A_0 = 10$ mm (dotted curve) and $A_0 = 5$ mm (solid curve). The initial amplitudes of the two solid curves are translated to match an amplitude of the same value on their respective dotted curves. The two displacement decays in Fig. 14a match well, suggesting that for $A_0 < 0$, the decay rate is not affected by different magnitudes of the initial amplitude. The same behavior was also observed in experiments with particles smaller in size (50 μm glass) and heavier in weight (1 mm steel) as well as in particle dynamics simulation using other $|A_0|$ values [20].

Fig. 14b shows that the displacement decays do not overlap for $A_0 > 0$ in contrast to that in Fig. 14a. This mismatch is caused by the discrepancy in the energy lost during the downstroke S3, compared with the downstroke S4. Although both strokes started with the same initial energy, more energy was lost during S3 than during S4 due to the same argument as that made for S1 and S2 earlier. Therefore, changes in the initial amplitude affect the displacement decay rate when $A_0 > 0$.

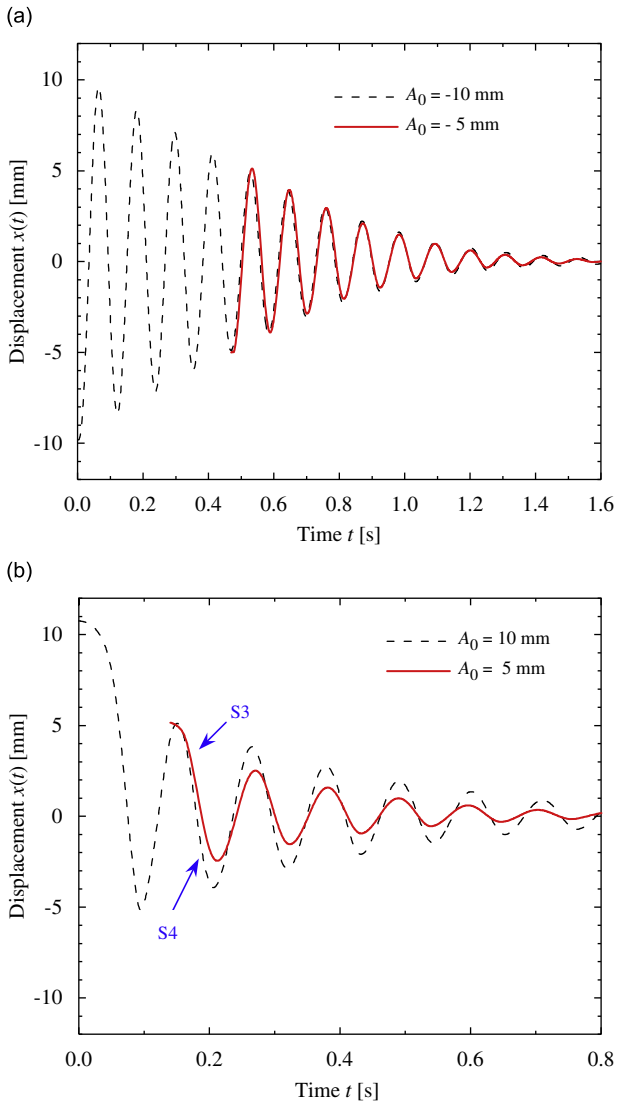

Fig. 14. Comparison of displacement decay between damping tests with initial amplitudes $A_0 = -10$ mm and $A_0 = -5$ mm (a), and between the tests with $A_0 = 10$ mm and $A_0 = 5$ mm (b) where S3 and S4 mark the two downstrokes.

5. Conclusions

This paper presents experimental demonstration and performance characteristics of an innovative particle-based thrust damping system for extreme temperature applications. The damping behavior of dry and uncharged particles of silica, glass and steel, ranging in size from nano-scale to macro-scale is examined. Experiments show that damping is temperature independent, repeatable over consecutive tests, and effective even at low excitation levels where particle-based impact damping fails. The displacement decay is non-linear and the damped frequency is greater than the undamped. Due to these two conditions, the damping behavior cannot be described by either a viscous or a frictional damping model.

In designing a damping system, the properties of the particles and parameters of the damping device should be carefully considered as they can impact the damping performance by influencing particle flow behavior, packing density and granular stress. The size, mass and surface characteristics of particles should be selected in order to maximize their flowability since free-flowing particles such as 1 mm diameter glass were observed to produce better damping in the thrust configuration than cohesive ones such as the 15 nm silica. The granular cohesive bond number Bo_g can be a useful indicator for such selection. The particle bed is shown to have an optimal value for its radius, below which piston jamming occurs and above which the size and mass of the device increase without providing additional damping. Damping rate is also sensitive to the piston's start position which is characterized by its immersion depth as well as the direction and magnitude of its initial amplitude. Displacement decay becomes faster with increasing piston immersion depth, greater damping is

produced when the displacements start from above the equilibrium position i.e. $A_0 > 0$, and the damping rate is not affected by the variation in the initial amplitude when $A_0 < 0$.

The experimental results also provide validation for particle dynamics based simulation models [20]. Practical applications of this damping method may be in military, aerospace and automotive industries that require damping with high reliability, under extreme temperature environments, and for a range of excitation levels.

Acknowledgments

This research was sponsored by the US Air Force Office of Scientific Research (Grant no. FA9550-05-1-0185/P00003) and supported by the US National Science Foundation IGERT program on Virtual Tribology at Northwestern University. The authors are grateful to Drs. B. L. Severson and K. Zhou as well as Profs. K.F. Ehmann, F.M. Borodich and J.M. Ottino for helpful discussions. LMK is grateful for partial support of a Royal Society, London travel grant to the University of Cardiff.

References

[1] C.W. De Silva, *Vibration Damping, Control, and Design*, Taylor & Francis, Boca Raton, 2007.
[2] M.A. Silveira, G.W. Brooks, D.J. Maglieri, *Results of an experimental investigation of small viscous dampers*, National Advisory Committee for Aeronautics, Washington DC, 1958.
[3] H.M. Jaeger, S.R. Nagel, Physics of the granular state, *Science* 255 (1992) 1523–1531.
[4] H.M. Jaeger, S.R. Nagel, R.P. Behringer, Granular solids, liquids, and gases, *Reviews of Modern Physics* 68 (1996) 1259–1273.
[5] J.J. Hollkamp, R.W. Gordon, Experiments with Particle Damping, San Diego, CA, pp. 2–12.
[6] X. Fang, H. Luo, J. Tang, Investigation of granular damping in transient vibrations using Hilbert transform based technique, *Journal of Vibration and Acoustics* 130 (2008) 031006.
[7] P. Lieber, D.P. Jensen, Acceleration damper: development, design, and some applications, *ASME Transactions* 67 (1945) 523–530.
[8] S.F. Masri, General motion of impact dampers, *The Journal of the Acoustical Society of America* 47 (1970) 229–237.
[9] N. Popplewell, S.E. Semercigil, Performance of the bean bag impact damper for a sinusoidal external force, *Journal of Sound and Vibration* 133 (1989) 193–223.
[10] A. Papalou, S.F. Masri, Performance of particle dampers under random excitation, *Journal of Vibration and Acoustics* 118 (1996) 614–621.
[11] A. Papalou, S.F. Masri, Response of impact dampers with granular materials under random excitation, *Earthquake Engineering & Structural Dynamics* 25 (1996) 253–267.
[12] R.D. Friend, V.K. Kinra, Particle impact damping, *Journal of Sound and Vibration* 233 (2000) 93–118.
[13] H.V. Panossian, Structural damping enhancement via non-obstructive particle damping technique, *Journal of Vibration and Acoustics* 114 (1992) 101–105.
[14] K.S. Marhadi, V.K. Kinra, Particle impact damping: effect of mass ratio, material, and shape, *Journal of Sound and Vibration* 283 (2005) 433–448.
[15] Z.W. Xu, K.W. Chan, W.H. Liao, An empirical method for particle damping design, *Shock and Vibration* 11 (2004) 647–664.
[16] M. Saeki, Impact damping with granular materials in a horizontally vibrating system, *Journal of Sound and Vibration* 251 (2002) 153–161.
[17] M. Saeki, Analytical study of multi-particle damping, *Journal of Sound and Vibration* 281 (2005) 1133–1144.
[18] C.X. Wong, M.C. Daniel, J.A. Rongong, Energy dissipation prediction of particle dampers, *Journal of Sound and Vibration* 319 (2009) 91–118.
[19] X. Fang, J. Tang, Granular damping in forced vibration: qualitative and quantitative analyses, *Journal of Vibration and Acoustics* 128 (2006) 489–500.
[20] X.-M. Bai, B. Shah, L.M. Keer, Q.J. Wang, R.Q. Snurr, Particle dynamics simulations of a piston-based particle damper, *Powder Technology* 189 (2009) 115–125.
[21] P.A. Cundall, O.D.L. Strack, Discrete numerical-model for granular assemblies, *Geotechnique* 29 (1979) 47–65.
[22] B.L. Severson, L.M. Keer, J.M. Ottino, R.Q. Snurr, Mechanical damping using adhesive micro or nano powders, *Powder Technology* 191 (2009) 143–148.
[23] T.R. Kreider, S.L. Hadden, Apparatus for damping vibration using macro particulates US Patent No. 6,955,250, 2005.
[24] E.M. Shtarkman, Dry viscous spring damper, US Patent No. 4,504,044, 1985.
[25] R.J. Monson, Passive collision damping device, US Patent No. 654,590 B1, 2003.
[26] J. Hovas, Shock absorber, US Patent No. 1,294,467, 1919.
[27] M.B. Stone, R. Barry, D.P. Bernstein, M.D. Pelc, Y.K. Tsui, P. Schiffer, Local jamming via penetration of a granular medium, *Physical Review E* 70 (2004) 041301.
[28] L.M. Keer, F.M. Borodich, B.M. Shah, Scaling and hierarchical structure of cohesive agglomerates of nanoparticles, in: F.M. Borodich, (Ed.), *IUTAM Symposium on Scaling in Solid Mechanics*, Cardiff, UK, Springer, 2007, pp. 287–297.
[29] A. Castellanos, The relationship between attractive interparticle forces and bulk behaviour in dry and uncharged fine powders, *Advances in Physics* 54 (2005) 263–376.
[30] J.N. Israelachvili, *Intermolecular and Surface Forces*, second ed., Academic, London, San Diego, 1992.
[31] K.M. Forward, D.J. Lacks, R.M. Sankaran, Methodology for studying particle-particle triboelectrification in granular materials, *Journal of Electrostatics* 67 (2009) 178–183.
[32] A.J. Forsyth, M.J. Rhodes, A simple model incorporating the effects of deformation and asperities into the Van der Waals force for macroscopic spherical solid particles, *Journal of Colloid and Interface Science* 223 (2000) 133–138.